Comprehending the influence of the particle size and stoichiometry on Al/CuO thermite combustion in close bomb: a theoretical study

Emilian Tichtchenko, Benoît Bédat, Olivier Simonin, Ludovic Glavier, David Gauchard, Alain Estève, Carole Rossi

Comprehending the influence of the particle size and stoichiometry on Al/CuO thermite combustion in close bomb: a theoretical study

Emilian Tichtchenko[a,c], Benoit Bedat[b], Olivier Simonin[b], Ludovic Glavier[c], David Gauchard[a], Alain Esteve[a], Carole Rossi[a]

[a]LAAS, University of Toulouse, CNRS-UPR 8001, France

[b] IMFT, University of Toulouse, CNRS-UMR 5502, France

[c] ArianeGroup SAS, 66 Route de Verneuil, 78130 Les Mureaux, France

Abstract

The paper is a theoretical exploration of complex Al/CuO thermite combustion processes, using a zero-dimensional (0D) model which integrates both condensed phase and gas phase reactions, and considers all thermodynamic stable molecular or atomic species identified during the Al+CuO reaction. We found that the particle size mainly influences the reaction kinetics and pressure development. Thermite with nano-sized particles (nanothermites) burns ~10 times faster than the same thermite with micron-sized particles (microthermites). This is due to the fact that the thermite reaction occurs mainly in condensed phase, i.e. in the melted Al phase, as all gaseous oxygens released by the CuO decomposition are spontaneously absorbed on the huge specific surface area of metallic Al. As a consequence, the pressure development in nanothermites follows the thermite chemical reaction, the gas phase is mostly composed of a metal vapor (mostly Cu and Al), Al suboxides, but is free of molecular oxygen. In contrast, when dealing with microthermites, an oxygen pressure peak occurs prior to the thermite reaction due to the gaseous O_2 released by the early CuO decomposition, that cannot be absorbed on the Al particles surface in real time. The powder stoichiometry greatly impacts the final pressure. Al lean thermites generate a higher final pressure (× 3) than stoichiometric and

Al rich mixtures, due to unreacted gaseous oxygen which remains in the gas phase after the full consumption of the metallic Al.

1. Introduction

Thermites composed of metallic reactant (mostly Al) coupled to an inorganic oxidizer (CuO, Fe_2O_3, Bi_2O_3, MoO_3 …) are non-explosive reactive materials which stay inert and stable until subjected to a sufficiently strong thermal stimulus, after which they undergo fast burning with release of high amount of chemical energy (up to 16 $kJ.cm^{-3}$). They represent an interesting class of energetics because of their high adiabatic flame temperature (> 2600 °C) [1,2] and tunable combustion properties. Indeed, a number of factors, in addition to the reactant (metal and metal oxide) nature and size, influence the combustion properties of these reactive materials. These additional factors include powder density, the thickness of the natural oxide layer that chemically passivates the particles, the stoichiometry (metal oxide over metal ratio) [3-8]. This tunability makes thermites promising in replacement of CHNO energetics for a large variety of applications such as propulsion [9], in-situ welding [10,11], material synthesis [12-13], generation of biocidal-agents [14,15], initiations [16-18], actuations in microsystems [19-22] and chips self-destruction [23-25]. Currently only general correlations between microscopic (particles size, stoichiometry…) and mesoscopic properties (powder compaction) of the thermite and its combustion behavior do exist, mostly derived from three decades of experimentations on thermite systems in research laboratories [26-28]. This study investigates theoretically the influence of two important microscopic parameters (particle size and stoichiometry) on the thermite combustion behavior in terms of combustion temperature, pressure development, gas phase composition and combustion residues. As a case study, an Al/CuO powdered thermite (mixture of Al and CuO particles) is considered because it is well-documented from both theoretical and experimental perspectives. Three Al/CuO systems are

considered: nanothermites (nT, with particles diameter equal to 100 nm), submicrothermites (sμT, with particles diameter equal to 0.7 μm), and microthermite (μT with particles diameter equal to 2 μm). The combustion of each Al/CuO system is simulated considering three stoichiometries: Al lean, stoichiometric and Al rich. To this end, we use an original multi-phasic zero-dimensional (0D) model that explicitly treats the energy and mass exchanges between the condense and gas phases. In addition, the model integrates an ensemble of chemical reactions, and physical transformations that are known to occur during the thermite reaction [29]. The detailed description of the model developed for thermite combustion prediction is outside the scope of this paper as it was already published [30]. Results not only confirm the experimental findings, e.g. the particles size mainly influences the reaction kinetics and pressure development, but importantly give an understanding of their underlying mechanisms. Nanothermites burns ~10 time faster than the microthermites because the oxidation of Al occurs mainly in the condensed phase, e.g. in the melted Al, as all gaseous oxygens released by the CuO decomposition are spontaneously absorbed by the melted Al particles. The temporal pressure evolution thus follows the thermite reaction and the gas phase is mostly composed of a metallic (Al and Cu) vapor. There is no gaseous Al suboxides and no gaseous oxygen. In contrast, in microthermites, an oxygen pressure peak occurs prior to the Al oxidation reaction as the oxygens released by the CuO decomposition cannot be all absorbed on the limited Al particles surface. The powder stoichiometry greatly impacts the final pressure. Al lean mixtures generate a higher final pressure (× 3) than stoichiometric and Al rich ones, due to unreacted gaseous oxygens which remain in the gas phase after full consumption of the metallic Al. Overall, this study, as the first theoretical exploration of complex thermite combustion processes, offers valuable guidelines for experimental investigations.

2. Computational details

The thermite system consists of a powder made of a homogeneous mixture of Al and CuO particles in a close chamber initially filled with ambient air. The Al particle purity (depending on the Al_2O_3 shell thickness), the powder density, the particles diameters (d_{Al} and d_{CuO}), and stoichiometric ratio (Al over CuO ratio, φ) define the main parameters of the system. To initiate the Al/CuO reaction, an input energy of 600 $kJ.kg^{-1}$ is injected uniformly (**Figure 1**).

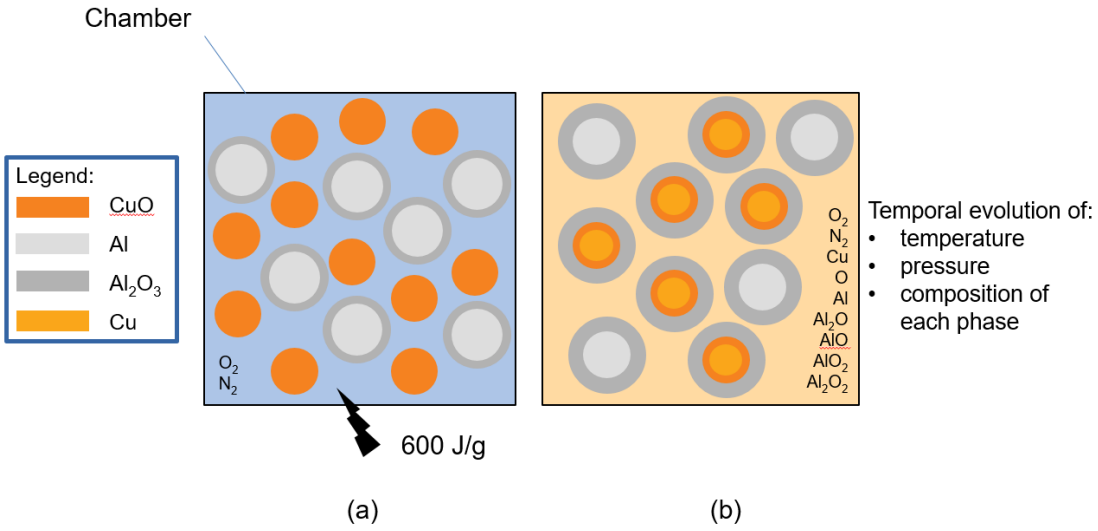

Figure 1. Schematic of the simulated thermite system: (a) initial system, (b) system during the thermite combustion.

The first key mechanism before the initiation of the thermite reaction is the CuO decomposition [31-35] releasing gaseous O_2. Then, oxygen species (either in atomic or molecular state) diffuse across the alumina shell to oxidize spontaneously metallic Al at the Al core/Al_2O_3 shell interface. This strong exothermic reaction relays the external supplied energy to complete thermite initiation and reach a steady state at the time defined as t_{steady}. Steady-state is defined as the moment when the temperature variation of each phase decreases below 10 $K.\mu s^{-1}$.

After the initiation, in addition to oxygen transport though Al_2O_3 growing layer followed by the oxidation of the melted Al as previously evoked, a wide range of mechanisms contribute to the self-sustained reaction. The chemical reaction and mass transfer mechanisms are listed in **Table**

1 with corresponding mathematical model and parameters. Energy transfers are summarized in **Table** 2. In addition to the heterogeneous reactions occurring in both gaseous and condensed phase, the model considers homogeneous reactions that take place only in the gaseous phase. Although no species transfer is considered between each particle phase, exchanged heat is modelled using a unit cell approach for the conduction and an enclosed assumption for the radiation.

Table 1*. List of chemical reaction and mass transfer mechanisms implemented to model the Al/CuO thermite initiation/combustion .c, g subscripts stand for condensed and gas, respectively.*

Reaction	**Mechanism**	**Mathematical implementation**
$2Al_{(c)} + 3/2O_{2(g)} \rightarrow Al_2O_{3(c)}$ $2Al_{(c)} + 3O_{(g)} \rightarrow Al_2O_{3(c)}$	Diffusion-reaction	Spalding quasi-steady state formulation/spontaneous reaction
$Al_2O_{3(c)} \rightarrow 2Al_{(g)} + 3/2O_{2(g)}$	Decomposition	Arrhenius dependence on temperature
$CuO_{(c)} \rightarrow Cu_{(c)} + 1/2O_{2(g)}$	Decomposition	Arrhenius dependence on temperature
$Cu_{(c)} \leftrightarrow Cu_{(g)}$	Evaporation/Condensation	Spalding quasi-steady state formulation/Clapeyron
$Al_{(c)} \leftrightarrow Al_{(g)}$	Evaporation/Condensation	Spalding quasi-steady state formulation/Clapeyron
$AlO_{x(c)}$ *reactions on condensed phases*	Detailed in [30]	Spalding quasi-steady state formulation/spontaneous reaction
Al, O, O_2, Al_2O, AlO, Al_2O_2, AlO_2	Reaction	Gas phase kinetics

Table 2*. List of heat transfer mechanisms implemented to model the Al/CuO thermite initiation/combustion.*

	Mechanism	**Mathematical implementation**
Particles - particles	Conduction	Unit cell approach taking into account the interstitial gas conductivity [36, 37]
	Radiation	Enclosed system approximation [38]

Particles - gas	Conduction	Steady-state formulation
	Radiation	Neglected

The model obeys the conventional mass and energy conservation equations (**Equations 1-4**), which are solved in the two distinct condensed phases, namely Al and CuO, and in the gas phase composed of Al, Cu, O, O_2, N_2, Al_2O, Al_2O_2, AlO, AlO_2.

The particles being considered uniformly distributed in the closed volume (**Figure 1**), a 0D approach is used to calculate the system temporal state evolution considering the mass and energy exchanges between Al, CuO particles and the gas as briefly summarized in subsections 2.1 and 2.2. All model details can be found in [30].

2.1. Mass and energy conservation in the condensed phases

$$N_k \frac{dm_{i,k}}{dt} = \sum_{r \in R} \dot{\omega}_{i,k}^{r} \quad (1)$$

$$N_k \frac{dH_k}{dt} = \sum_{k' \neq k} Q_{k' \to k} + Q_{init} \quad (2)$$

where N_k is the number of particles in a given phase *k* (*k* = Al, CuO); $m_{i,k}$ is the mass of the species *i* in the particle *k* and $\dot{\omega}_{i,k}^{r}$ is the reaction rate of the species *i* from reaction *r* relative to particle *k*; H_k is the enthalpy of one particle of the particle phase *k*, assuming that all the particles within a given phase *k* are at the same temperature, and, integrating liquid to solid phase transformation; $Q_{k' \to k}$ is the heat flux received by a given particle phase *k* from either the other particle phase or the gas, noted *k'*. Q_{init} is the input energy per unit of time used to ignite the self-sustained reaction. Heat fluxes are symmetric, hence for any condensed or gaseous phase *k'* and k, $Q_{k' \to k} = -Q_{k \to k'}$

2.2 Mass and energy conservation in the gas phase

$$\frac{dm_g}{dt} = \sum_{r \in R} \sum_i \dot{\omega}_{i,g}^{r} = \Gamma_g \quad (3)$$

$$\frac{d}{dt}\left(m_g Y_{i,g}\right) = \sum_{r \in R} \dot{\omega}_{i,g}^{r} \quad (4)$$

$$\frac{d}{dt}\left(m_g u_g\right) = \sum_{k=p,q} Q_{k \to g} \quad (5)$$

where $\dot{\omega}_{i,g}^{r}$ and Γ_g are the gas production rate of the species *i* and the total mass flux going from all the particles to the gas, respectively; $Y_{i,g}$ is the mass fraction of the species i; u_g is the specific total internal energy (summing all species contribution) of the gas at the overall gas temperature; $Q_{k\to g}$ is the energy fluxes received by the gas from the particle phase *k*. m_g is the mass of the gas phase.

2.3. Gas phase kinetics

We consider the gas phase kinetics based on the scheme by Catoire et al. [39] from which only the reactions involving Al and O species are considered. **Table 3** lists the gas phase reactions along with their kinetic parameters. The open-source tool Cantera dedicated to rate theory calculations was used to solve the set of differential equations associated with the gas phase reactions [40]. Finally, the gas transport properties were computed based on the Lennard-Jones potential using Cantera considering parameters found in the literature.

Table 3. *Gas phase chemical reactions and kinetic parameters, defined as* $AT^n e^{-B/T}$ [41]. *X corresponds to the gas phase species: Al, Cu, O, O_2, Al_2O, AlO, Al_2O_2, AlO_2, N_2.*

Chemical reaction	**A (cm^{-3}× mol^{-1}× s^{-1})**	***B* (K)**	n
$Al + O_2 \leftrightarrow AlO + O$	9.7×10^{13}	80.5	0
$AlO + O_2 \leftrightarrow AlO_2 + O$	4.6×10^{14}	10008	0
$Al_2O_2 \leftrightarrow AlO + AlO$	1.0×10^{15}	59335	0
$Al_2O_2 \leftrightarrow Al + AlO_2$	1.0×10^{15}	74937	0
$Al_2O_2 \leftrightarrow Al_2O + O$	1.0×10^{15}	52466	0
$AlO_2 \leftrightarrow AlO + O$	1.0×10^{15}	44564	0
$Al_2O \leftrightarrow AlO + Al$	1.0×10^{15}	67035	0
$Al + O + X \leftrightarrow AlO + X$	3.0×10^{17}	0	-1
$O_2 + X \leftrightarrow O + O + X$	1.2×10^{14}	54244	0

2.4. Physical and kinetic parameters

All thermodynamic data, for condensed and gaseous species, are taken from JANAF tables [42] and NASA7 polynomials [43]. The kinetics of CuO, Al_2O_3 decomposition and oxygen species diffusion follows a single Arrhenius dependence on temperature. The Arrhenius parameters, activation energy, and pre-exponential factor are critical to correctly predict the combustion kinetics, despite the fact that the decomposition mechanisms for both materials are still not well characterized nor fully quantified. For CuO, the prefactor k_0 and the activation energy E_a are fitted such as the decomposition of copper oxide happens between 800 K and 1200 K [44, 45]. The oxygen diffusion is also thermally activated following an Arrhenius law, with prefactor k_0 and activation energy E_a fitted using experimental data [26]. Finally, vaporization/condensation of Al and Cu are treated based on the gas/liquid equilibrium and Spalding formulation. Their vaporization points evolve with respect to the pressure as a function of a Clapeyron law.

3. Results and discussion

Three different sizes of Al and CuO particles were investigated: $d_{CuO} = d_{Al} = 100$ nm (noted as nT), $d_{CuO} = d_{Al} = 700$ nm (noted as sμT), and, $d_{CuO} = d_{Al} = 4$ μm (noted as μT). A constant alumina shell thickness of 4 nm coats the Al particles, whatever their particles' size. This gives an Al purity of 0.7, 0.95, 0.99 for nT, sμT and μT, respectively. For each thermite (nT, sμT, μT), three equivalence ratios (φ, **Equation 6**) are considered: 0.8 (fuel lean), 1 (stoichiometric), 1.5 (fuel rich).

$$\varphi = \frac{81 \times m_{pureAl}}{160 \times m_{CuO}} \qquad (6)$$

Finally, the powder density is set at 50 % of the theoretical density of Al/CuO thermite. The theoretical density of the nT system is 2686, 2598, 2431 kg.m^3 for φ = 0.8, 1 1.5 respectively. For each powder, the total (S_{tot}) and aluminum (S_{Al}) surface area per volume of powder is reported in **Table 4**.

Table 4. *Total (S_{tot}) and aluminum (S_{Al}) surface area per volume of powder, and pressurization rate, for nT, sµT, and µT.*

Thermite system	**nT**	**sµT**	**µT**
S_{tot} ($km^2.m^{-3}$)	30	4	0.75
S_{Al} ($km^2.m^{-3}$)	12.13	1.5	0.26
Pressurization rate ($MPa.\mu s^{-1}$)	65	88	34

3.1. Dominant role of Al particle surface area on the combustion regime and pressure development

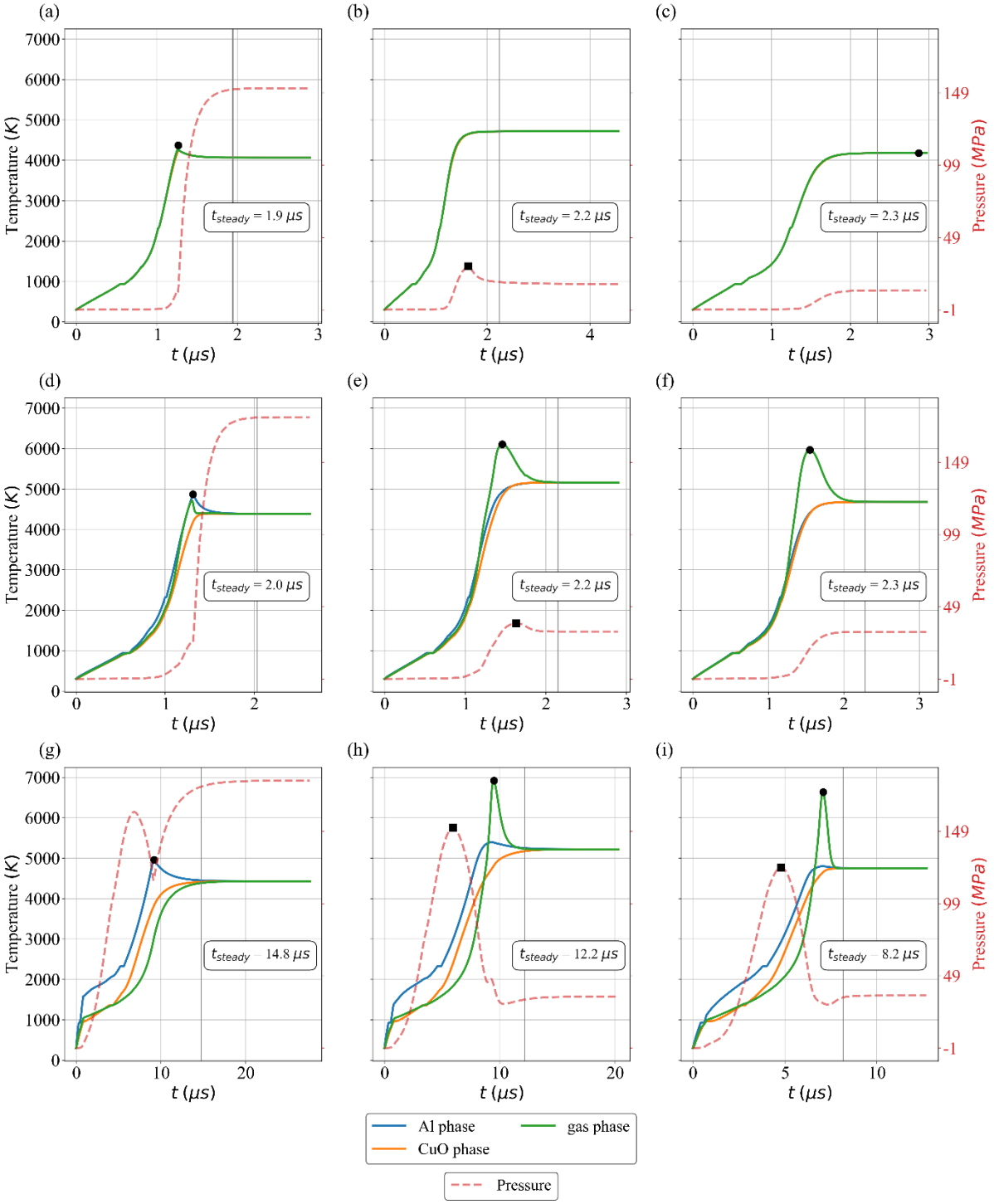

Figure 2. Pressure (dotted lines) and temperature (solid lines) temporal evolution of each phase i.e. gas, Al and CuO particles for the three thermite systems: nT (a) Al lean, (b) stoichiometric, (c) Al rich; sμT (d) Al lean, (e) stoichiometric, (f) Al rich; μT (g) Al lean, (h) stoichiometric, (i) Al rich. Note that if only a green line is visible, it means that the three phases are evolving

at the same temperature. ● and ■ represent the maximum temperature and maximum pressure of the gas. The vertical grey line corresponds to the beginning steady-state combustion.

Graphs in **Figure 2 a-c** plot the temperature and pressure time evolution for each phase, namely gas, Al, and, CuO and for each considered Al/CuO systems: nT, sμT, and μT.

Temperature evolution. In the temperature temporal curve (orange, blue and green curves in **Figure 2**), we can distinguish the preheating stage during which the temperature increases linearly due to the application of the input energy, followed by an abrupt temperature rise corresponding to the thermite combustion before reaching a final plateau at 4700, 5160 and 5219 K as no thermal losses are considered in our simulation. Clearly a stationary regime is reached once all the reactions are completed. The time to reach this stationary regime (t_{steady} in **Figure 2**) increases with the particle size, explained by the difference in the Al specific surface area. Considering stoichiometry powder (**Figure 2b, e, h**), it is ~2.2 μs for the nT system and rises up to 12.2 μs for the μT.

Interestingly, while in the nT, all three phases are thermalized (i.e. evolving at the same temperature) during the different combustion steps, they do not in sμT and μT. In these two latter systems, the gas phase heats up faster and reaches a higher temperature (~ ● in **Figure 2e, f, h, i,** reaching + 1000 K in some specific conditions**)** than the Al and CuO phases. In addition, μT features a singular thermal behavior compared to nT and sμT. The particle being micrometric, interfacial or surface area is only 0.75 $km^2.m^{-3}$ (40 times less than that of nT) impeding the Al and CuO particles thermalization and explaining why each evolves at a distinct temperature. As expected, the Al heats up faster during the initiation stage because the reaction initiates in the core Al particles. Noteworthy a slight overtemperature peak is observed in the Al phase pointing to the Al and gas phase interplay during the reaction: the gas heats the aluminum particles before the different Al suboxides condensate through an endothermic reaction on both particles, and thus decreasing the temperature until reaching the

thermodynamic equilibrium. On the contrary, the CuO phase heating is delayed in time, as the endothermic decomposition reaction slows down its temperature rise. In µT (φ = 1 and 1.5), the gas phase overtemperature peak reaches ~ + 2000 K compared to the condensed phase temperatures (**Figure 2h, i**, green curve).

Pressure development. Considering now the pressure curves (dotted lines in **Figure 2**), and considering stoichiometric mixture **(Figure 2b, e, h**) a final pressure of 19, 32 and 35 MPa is obtained for nT, sµT and µT, respectively. The differences are simply due to the differences in Al particle purity from one system to another, as the final pressure with heat losses is only function of the thermodynamic properties of the mixture, and independent of the particle size. Importantly, we observe two major differences in the pressure development between µT and the two other thermites. First, the pressurization rate obtained for nT and sµT systems is 8 times superior to those of poorly-reactive µT, which agrees with the experimental findings pointing to higher reactivity of nanothermites [46, 47] due to the enhanced interfacial contact between condensed and gas phases compared to that of the microscale mixtures. Second, the µT features a pressure peak at ~150 MPa before the thermite combustion. Interestingly, the oxygen released by the CuO decomposition between 600 – 1200 K is not consumed readily in time on the Al particles to further react with metallic Al core, as the Al particle surface area is limited to 0.26 $km^2.m^{-3}$ only. This is also characterized by the time evolution of the O_2 pressure in the gas phase in **Figure 3,** considering only stoichiometric systems (nT, sµT and µT taken at φ=1). The surface area not only allows for faster thermalization of the different phases as discussed in the previous paragraph, but also greatly impacts the kinetic of absorption of reactive species such as O_2 from the gas phase to the Al particles through condensation mechanisms. In nT, the oxygen released by the CuO decomposition, starting ~ 600 K, is consumed almost spontaneously by the high Al particle surface (S_{Al}=12.13 $km^2.m^{-3}$, **Table 4**) and redox reaction occurs in the Al particles (**Figure 3,** dotted curve). In sµT, the oxygen released by the CuO

decomposition is also consumed to react with Al in the Al phase (S_{Al}=1.5 $km^2.m^{-3}$, **Table 4**) but with a slight delay (oxygen peak ■ in **Figure 2b, e, h, i** curves). But, in µT, the gaseous oxygens cannot be consumed and thus reacts in the gas phase with vaporized Al.

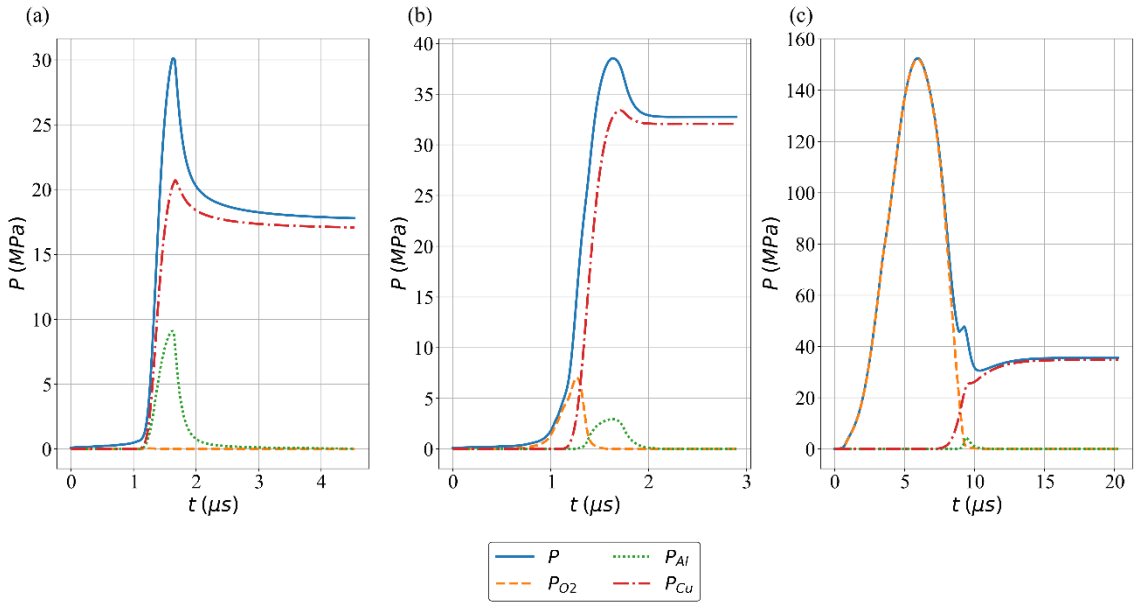

Figure 3. Total pressure (solid blue), copper pressure (dotted red), aluminum pressure (dotted green) and oxygen pressure (dotted orange) temporal evolution for stoichiometric nT (a), sµT (b), and µT (c).

Gas phase composition. The gas phase composition during the different steps of the combustion is given in **Figure 4** for each thermite, nT, sµT and µT taken at φ=1. Initially, only oxygen and nitrogen are present in the gas phase, according to a standard dry atmospheric condition. When temperature approaches the boiling temperature of aluminum, evaporation increases and reacts with gaseous oxygens producing AlO_x intermediates: a majority of AlO, but also Al_2O. It has to be noted that Al_2O_2 is in anecdotic proportion. We observe first the formation of AlO, followed by O and Al_2O which might originate from the progressive gas phase enrichment with atomic Al during its vaporization. Al_xO_y sub-oxides also condensate on Al and CuO particles as the reaction goes to completion. Gaseous Cu appears in the gas phase when temperature

tends to its boiling point depending on pressure conditions. The gas phase composition greatly varies between nT and the two other systems: the gas phase of the nT contains almost no aluminum suboxide. As the oxygen is instantaneously absorbed on the huge aluminum particle surface (12.13 $km^2.m^{-3}$), there is no oxygen in the gas phase to react with Al vapor when this latter starts to vaporize. In addition, the aluminum suboxides formed by the oxidation reaction directly condense onto both particles, again due to the high specific surface of the particles (30 $km^2.m^{-3}$). By contrast, for µT and sµT systems, the total gaseous mass fraction of Al_xO_y reach up to 20% and 26% respectively, and are present during at least one microsecond.

Final products analysis. Finally, the chemical composition and the particle sizes of the final products are analyzed for each thermite system. Similar trends are observed for the three systems (**Table 5)**, e.g. Al particles increase in size (by 5% for nT and 8% for µT) and get fully oxidized in Al_2O_3. CuO particles decrease in size by roughly 10 % leaving a majority of pure copper on which a non-negligible amount of aluminum oxide is formed through the condensation of Al suboxides.

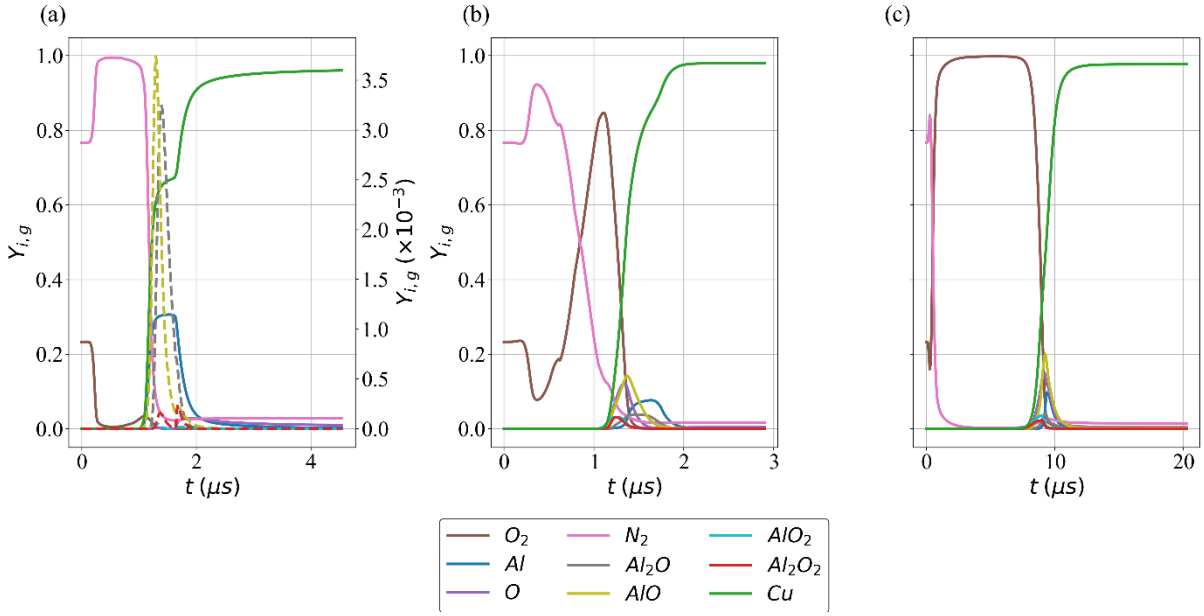

Figure 4. Gas phase species temporal evolution for stoichiometric nT (a), sµT (b), and, µT (c).

Table 5*. Physico-chemical characteristics of the combustion residues of stoichiometric nT (a), sμT (b), and, μT (c).*

Thermite system	**nT**	**sμT**	**μT**
Mass percentage of pure Cu in CuO particle (in %)	96	95	99.3
Mass percentage of Al_2O_3 in final alumina particle	99	99	100
Mass percentage of Al_2O_3 on final Cu particle	4	5	0.7
Final Al_2O_3 particles mean diameter (nm)	104	740	4340
Final Cu particles mean diameter (nm)	84	600	3300
Initial d_{Al} and d_{CuO} (nm)	100	700	4000

3.2 Key role of thermite stoichiometry (equivalence ratio) on the final pressure

For each 9 Al/CuO systems, e.g. stoichiometric nT, sμT, μT, Al rich nT, sμT, μT and Al poor nT, sμT, μT, **Table 6** summarizes the simulation results in terms of pressurization rate, pressure pre-peak, final pressure, temperature and time to reach the steady-state combustion regime. The pressure and temperature time evolution curves for each phases and thermite systems are plotted in **Figure 5**.

Table 6. *Summary of simulated combustion characteristics (pressurization rate, pressure, temperature and time delay to reach the steady state) as a function of equivalence ratio (φ) and for the three thermite systems: nT, sμT and μT.*

Thermite system	**nT**			**sμT**			**μT**		
φ	0.8	1	1.5	0.8	1	1.5	0.8	1	1.5
Pressurization rate (MPa/μs)	399	65	26	530	88	68	32	34	47
Final Temperature (K)	4065	4717	4178	4387	5161	4680	4430	5220	4748

Final Pressure (MPa)	153	18	14	181	33	33	185	36	36
Pre-peak Pressure (MPa)	No	30	No	No	39	No	No	152	125
t_{steady} (µs)	1.9	2.2	2.3	2	2.2	2.3	14.8	12.2	8.2
S_{Al} (km^2. m^{-3}) as reminder	10.6	12.1	15.1	1.3	1.5	1.9	0.2	0.3	0.3

Clearly, the equivalence ration affects the combustion behavior and characteristics (**Table 6** and **Figure 2)**: in particular, the lack of Al in the mixtures leads to an excess of oxygens released in the gas phase, explaining why the final pressure of all Al lean mixtures is × 5 those of others. The final pressure for φ = 0.8 is in the 150 - 185 MPa range whatever the thermite systems, while it is < 40 MPa for φ = 1 and 1.5. µT systematically produces the pressure peak prior the steady state due to oxygens release as discussed in the preceding section. The intensity of these oxygen pre-peaks increases with decreasing the stoichiometry (from 152 MPa to 125 MPa for φ=1 to 1.5) as Al surface (S_{Al}) on which O_2 is absorbed increases with φ as summarized in **Table 6**. µT systems reach their steady state within ~10 µs: 8 µs for Al rich and 15 µs for Al lean. Considering nT and sµT systems, a much faster initiation and combustion regime is observed, as the time needed to reach the steady state falls within 2 – 2.3 µs. Interestingly, the steady state is reached faster when reducing the Al content (φ = 0.8). In contrast, µT system behaves oppositely as it features a higher reactivity for higher Al content (φ = 1.5), because of the increase of aluminum specific surface area.

It is also interesting to note that for both nT and sµT, there is an anecdotic oxygen pressure pre-peak (30 and 39 MPa) at φ = 1, which is not present for Al lean and Al rich mixtures. This pressure overshot is explained by the fact that aluminum which is vaporized and reacts in the gas to form aluminum suboxide, prior the condensation of these latter on particles. In the Al lean and Al rich mixtures, the energy is not sufficient to permit enough aluminum to vaporize

to observe this phenomena. Regarding final combustion temperature, stoichiometric mixtures are systematically ~600 K higher than those of Al rich and lean ones due to a higher heat of reaction of the mixture. Typically, the heat of reaction of is of 3381 $kJ.kg^{-1}$, 4071 $kJ.kg^{-1}$, 3728 $kJ.kg^{-1}$ for φ = 0.8, 1 and 1.5, respectively.

The temperature profiles of each phase (Al, CuO and gas) during the combustion are particularly interesting to analyze from **Figure 2** curves. In µT thermite system, whatever φ, each phase behaves thermally differently: the temperature of Al particles rises first as the thermite reaction occur into them, and noteworthy the highest Al phase temperature is obtained for φ = 1 (5220 K). Then, when all the core particle aluminum is fully oxidized (at t = 9 µs), the temperature of the Al phase decreases as the heat is transferred to the gas and copper oxide particles. This is the reason why CuO particle temperature rises after the Al ones for all µT systems. Gas phase is the third to heat up but, because of the excess in oxygen in the gas phase (pressure pre-peak), the temperature of the gas increases suddenly once Al is vaporized, giving birth to gas phase exothermic reactions, which occurs only for φ = 1 and 1.5, as Al lean system has no enough Al to induce gas phase reactions.

In stoichiometric and Al rich sµT systems, both the CuO and Al condensed phases are almost thermalized whereas the gas heats up faster (● in **Figure 2 e-f)**). However, in Al lean sµT, the Al and gas phases heat up faster than the CuO phase as indicated by the overtemperature peak (● in **Figure 2 g**).

3.3. Influence of gas phase treatment: kinetic theory vs thermodynamic equilibrium

For calculations presented in section 3.1 and 3.2, we used kinetic theory of gases based on the molecular interactions, which leads to the macroscopic relationships detailed in the computational section. Considering that the molecular chemical processes in the gas phase should be fast compared to condensed phases processes limited by the atomic mass transport, it is legitimate to wonder if it is necessary to solve the differential rate equations of the

molecular reactions or replacing it by a gas phase equilibrium determination, as already used in [48]. This section aims at discussing this point. For that purpose, we simulated the combustion of the 3 stoichiometric Al/CuO systems, nT, sμT and μT, considering the gas phase at the equilibrium and we compared the combustion temperature, pressurization rate, maximum pressure and gaseous composition with those obtained in section 3.1 for which a kinetic treatment was considered for the gas phase. No difference is observed for μT and sμT (**Figure 5)** so that assumption of gaseous equilibrium can be done for particle size smaller than 0.7 nm. For μT and sμT, the global reaction characteristic time can be considered longer than gaseous molecular reaction time. However, in nT, the gaseous composition temporal evolution differs both in the amount and temporal distribution of gaseous species that are in minority (mass ratio $< 10^{-2}$). Assuming the gas at the equilibrium, AlO appears first and and is the dominant species among other Al suboxide species in the gas phase which can be considered as inexistent. AlO is similarly present using the kinetic algorithm, but is followed by Al_2O in almost the same quantity (3×10^{-2} mass ratio in **Figure 5d**). Therefore, the equilibrium assumption is not fully valid for nT system as the characteristic time of the different interphase mechanisms decreases to fall in the order of magnitude of the gaseous kinetics characteristic time scale. However, the impact of this assumption on the global behavior of the total system, even in nT systems, is negligible.

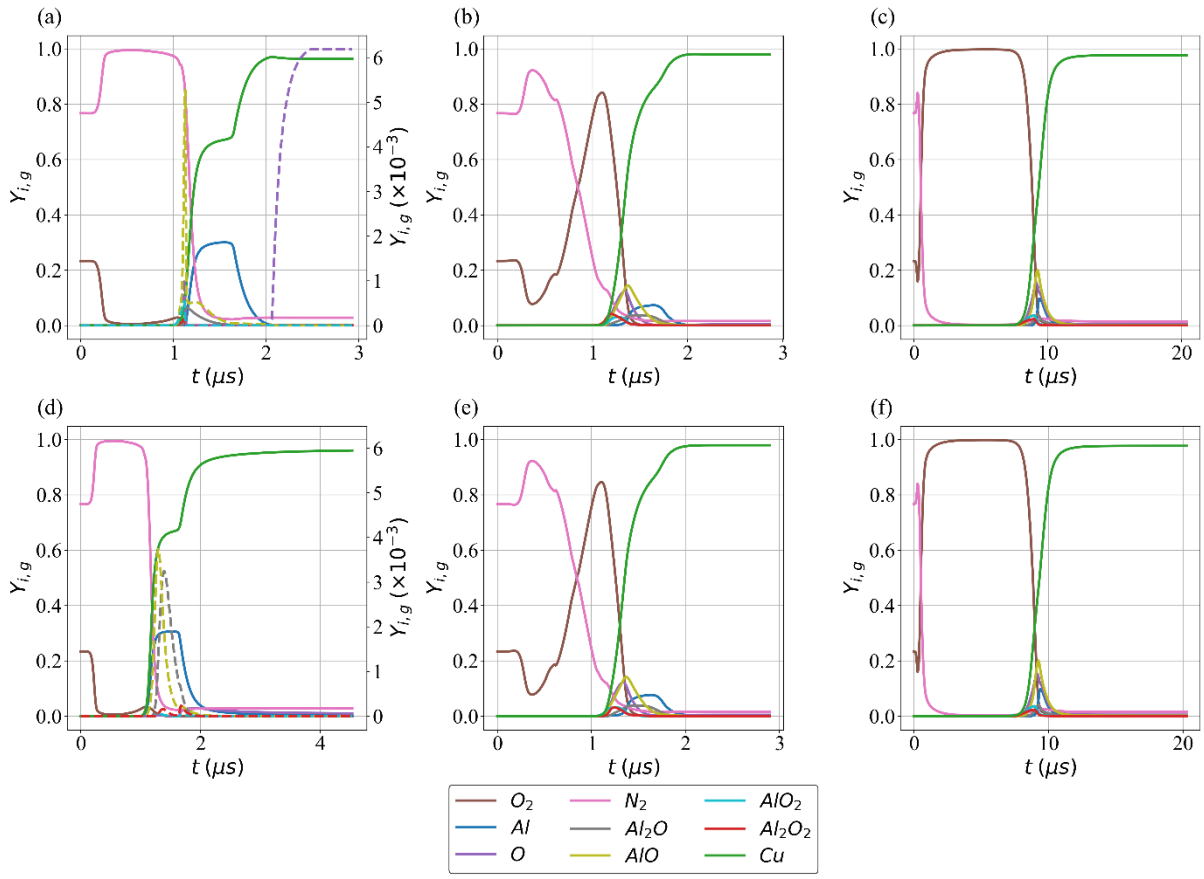

Figure 5. Time evolution of the gas phase species ($Y_{i,g}$) for stoichiometric nT (a,d), sμT (b,e), and, μT (c,f) using the equilibrium approximation (top) and the gas phase kinetic approach (bottom).

3. Concluding remarks

We theoretically investigated the influence of two microscopic parameters, the particle size and mixture stoichiometry, on Al/CuO powdered thermite combustion. We detailed and analyzed the temperature, pressure, gas phase composition temporal evolution, and, combustion residues. Three Al/CuO systems were considered: nanothermites (nT, with particles diameter equal to 100 nm), submicrothermites (sμT, with particle diameter equal to 0.7 μm), and microthermite (μT with particle diameter equal to 4 μm). For each, three stoichiometries were simulated (Al lean, stoichiometric and Al rich) using a multi-phasic 0D combustion model integrating chemical reactions in both condensed and gas phases, and typical physical transformations occuring during the thermite reaction. Nanothermites burns ~10 time faster than the

microthermites because the oxidation of Al occurs mainly in the melted Al, as all gaseous oxygens released by the CuO decomposition are spontaneously absorbed onto the high surface area of melted Al particles. The temporal pressure evolution follows the thermite reaction and the gas phase is mostly composed of a metallic (Al and Cu) vapor. No Al suboxides and oxygen are present. In contrast, in microthermites, an oxygen pressure peak occurs prior to the Al oxidation reaction as the oxygens released by the CuO decomposition cannot be all absorbed on the Al particles surface. The powder stoichiometry greatly impacts the final pressure. Indeed, Al lean mixtures generate a higher final pressure (× 5) than stoichiometric and Al rich ones, due to unreacted gaseous oxygens which remain in the gas phase after the full consumption of the metallic Al.

Acknowledgements

The authors grateful acknowledge support from the European Research Council (H2020 Excellent Science) Researcher Award (grant 832889 – PyroSafe). The authors also thank Elliott Pollice for his help in implementing the gas phase kinetic in the model.

References

[1] S. H. Fischer, M. C. Grubelich, Theoretical energy release of Thermites, Intermetallics, and Combustible Metals, https://www.osti.gov/servlets/purl/658208. doi:10.2172/658208.

[2] S. Kabra, S. Gharde, P. M. Gore, S. Jain, V. H. Khire, B. Kandasubramanian, Recent trends in nanothermites: Fabrication, characteristics and applications, *Nano Express*, **2020**, *1* (3). doi: 10.1088/2632-959X/abbce7.

[3] M. Polis, A. Stolarczyk, K. Glosz, T. Jarosz, Quo Vadis, Nanothermite? A Review of Recent Progress, *Materials*, **2022**, *15* (9). doi: 10.3390/ma15093215.

[4] T. Wu, G. Lahiner, C. Tenailleau, B. Reig, T. Hungria, A. Esteve, C. Rossi, Unexpected enhanced reactivity of aluminized nanothermites by accelerated aging, *Chem Eng J*, **2021**, *418*, 129432. doi: 10.1016/j.cej.2021.129432.

[5] Y. J. Chen, W. Ren, Z. L. Zheng, G. G. Wu, B. Hu, J. H. Chen, J. X. Wang, C. P. Yu, K. F. Ma, X. L. Zhou, W. C. Zhang, Reactivity adjustment from the contact extent between CuO and Al phases in nanothermites, *Chem Eng J*, **2020**, *402*, 9. doi: 10.1016/j.cej.2020.126288.

[6] R. Ramachandran, V. S. Vuppuluri, T. J. Fleck, J. F. Rhoads, I. E. Gunduz, S. F. Son, Influence of Stoichiometry on the Thrust and Heat Deposition of On-Chip Nanothermites, *Propell Explos Pyrot*, **2018**, *43* (3), 258-266. doi: 10.1002/prep.201700132.

[7] J. Zapata, A. Nicollet, B. Julien, G. Lahiner, A. Esteve, C. Rossi, Self-propagating combustion of sputter-deposited Al/CuO nanolaminates, *Combust Flame*, **2019**, *205*, 389-396. doi: 10.1016/j.combustflame.2019.04.031.

[8] S. Palussiere, J. Cure, A. Nicollet, P. Fau, K. Fajerwerg, M. L. Kahn, A. Esteve, C. Rossi, The role of alkylamine in the stabilization of CuO nanoparticles as a determinant of the Al/CuO redox reaction, *Phys Chem Chem Phys*, **2019**, *21* (29), 16180-16189. doi: 10.1039/c9cp02220a.

[9] C. S. Staley, K. E. Raymond, R. Thiruvengadathan, S. J. Apperson, K. Gangopadhyay, S. M. Swaszek, R. J. Taylor, S. Gangopadhyay, Fast-Impulse Nanothermite Solid-Propellant Miniaturized Thrusters, *J Propul Power*, **2013**, *29* (6), 1400-1409. doi: 10.2514/1.B34962.

[10] D. M. B. Dombroski, A. Q. Wang, J. Z. Wen, M. Alfano, Joining and welding with a nanothermite and exothermic bonding using reactive multi-nanolayers - A review, *J Manuf Process*, **2022**, *75*, 280-300. doi: 10.1016/j.jmapro.2021.12.056.

[11] A. J. Swiston, E. Besnoin, A. Duckham, O. M. Knio, T. P. Weihs, T. C. Hufnagel, Thermal and microstructural effects of welding metallic glasses by self-propagating reactions in multilayer foils, *Acta Mater*, **2005**, *53* (13), 3713-3719. doi: 10.1016/j.actamat.2005.04.030.

[12] L. J. Groven, J. A. Puszynski, Combustion synthesis and characterization of nickel aluminide-carbon nanotube composites, *Chem Eng J*, **2012**, *183*, 515-525. doi: 10.1016/j.cej.2011.12.070.

[13] C. Farley, T. Turnbull, M. L. Pantoya, E. M. Hunt, Self-propagating high-temperature synthesis of nanostructured titanium aluminide alloys with varying porosity, *Acta Mater*, **2011**, *59* (6), 2447-2454. doi: 10.1016/j.actamat.2010.12.044.

[14] F. Y. Xu, P. Biswas, G. Nava, J. Schwan, D. J. Kline, M. C. Rehwoldt, L. Mangolini, M. R. Zachariah, Tuning the reactivity and energy release rate of I2O5 based ternary thermite systems, *Combust Flame*, **2021**, *228*, 210-217. doi: 10.1016/j.combustflame.2020.12.047.

[15] X. H. Liu, M. Schoenitz, E. L. Dreizin, Preparation, ignition, and combustion of magnesium-calcium iodate reactive nano-composite powders, *Chem Eng J*, **2019**, *359*, 955-962. doi: 10.1016/j.cej.2018.11.091.

[16] C. Rossi, Engineering of Al/CuO Reactive Multilayer Thin Films for Tunable Initiation and Actuation, *Propellants, Explosives, Pyrotechnics*, **2019**, *44* (1), 94-108. doi: 10.1002/prep.201800045.

[17] S. Fu, R. Q. Shen, P. Zhu, Y. H. Ye, Metal-interlayer-metal structured initiator containing Al/CuO reactive multilayer films that exhibits improved ignition properties, *Sensor Actuat a-Phys*, **2019**, *292*, 198-204. doi: 10.1016/j.sna.2019.04.019.

[18] J. L. Pouchairet, C. Rossi, PyroMEMS as Future Technological Building Blocks for Advanced Microenergetic Systems, *Micromachines (Basel)*, **2021**, *12* (2). doi: 10.3390/mi12020118.

[19] L. Salvagnac, S. Assie-Souleille, C. Rossi, Layered Al/CuO Thin Films for Tunable Ignition and Actuations, *Nanomaterials (Basel)*, **2020**, *10* (10). doi: 10.3390/nano10102009.

[20] S. Suhard, P. Fau, B. Chaudret, S. Sabo-Etienne, M. Mauzac, A. F. Mingotaud, G. Ardila-Rodriguez, C. Rossi, M. F. Guimon, When Energetic Materials, PDMS-Based Elastomers, and Microelectronic Processes Work Together: Fabrication of a Disposable Microactuator, *Chem Mater*, **2009**, *21* (6), 1069-1076. doi: 10.1021/cm803146y.

[21] G. A. A. Rodriguez, S. Suhard, C. Rossi, D. Esteve, P. Fau, S. Sabo-Etienne, A. F. Mingotaud, M. Mauzac, B. Chaudret, A microactuator based on the decomposition of an energetic material for disposable lab-on-chip applications: fabrication and test, *J Micromech Microeng*, **2009**, *19* (1). doi: 10.1088/0960-1317/19/1/015006.

[22] D. A. de Koninck, F. Molina-Lopez, D. Briand, N. F. de Rooij, Foil-Level Inkjet-Printed pyroMEMS Balloon Actuators: Fabrication, Modeling, and Validation, *J Microelectromech S*, **2014**, *23* (6), 1417-1427. doi: 10.1109/JMEMS.2014.2314702.

[23] S. S. Pandey, N. Banerjee, Y. Xie, C. H. Mastrangelo, Self-Destructing Secured Microchips by On-Chip Triggered Energetic and Corrosive Attacks for Transient Electronics, *Adv Mater Technol-Us*, **2018**, *3* (7). doi: 10.1002/admt.201800044.

[24] X. Ma, S. Gu, Y. Li, J. Lu, G. Yang, K. Zhang, Additive-Free Energetic Film Based on Graphene Oxide and Nanoscale Energetic Coordination Polymer for Transient Microchip, *Adv. Funct. Mater.* **2021**, 2103199. doi: 10.1002/adfm.202103199.

[25] F. Sevely, T. Wu, F. Sodre Ferreira de Sousa, L. Seguier, V. Brossa, S. Charlot, A. Esteve and C. Rossi, Developing a highly responsive miniaturized security device based on a printed copper ammine energetic composite, *Sensor Actuat a-Phys*, **2022**, *346*, *113838.* doi: 10.1016/j.sna.2022.113838.

[26] L. Glavier, G. Taton, J. M. Ducere, V. Baijot, S. Pinon, T. Calais, A. Esteve, M. D. Rouhani, C. Rossi, Nanoenergetics as pressure generator for nontoxic impact primers: Comparison of Al/Bi2O3, Al/CuO, Al/MoO3 nanothermites and Al/PTFE, *Combust Flame*, **2015**, *162* (5), 1813-1820. doi: 10.1016/j.combustflame.2014.12.002.

[27] A. Williams, I. Shancita, I. Altman, N. Tamura, M. L. Pantoya, On the Pressure Generated by Thermite Reactions Using Stress-Altered Aluminum Particles, *Propell Explos Pyrot*, **2021**, *46* (1), 99-106. doi: 10.1002/prep.202000221.

[28] K. S. Martirosyan, Nanoenergetic Gas-Generators: principles and applications, *J Mater Chem*, **2011**, *21* (26), 9400-9405. doi: 10.1039/C1JM11300C.

[29] V. Baijot, L. Glavier, J. M. Ducere, M. D. Rouhani, C. Rossi, A. Esteve, Modeling the Pressure Generation in Aluminum-Based Thermites, *Propell Explos Pyrot*, **2015**, *40* (3), 402-412. doi: 10.1002/prep.201400297.

[30] E. Tichtchenko, V. Folliet, O. Simonin, B. Bedat, L. Glavier, A. Esteve, C. Rossi, Combustion model for thermite materials integrating explicit and coupled treatment of condensed and gas phase kinetics, *Proc. Combust. Inst.*,**2022**, *1-9*. doi: 10.1016/j.proci.2022.08.117.

[31] F. Yi, J. B. DeLisio, N. Nguyen, M. R. Zachariah, D. A. LaVan, High heating rate decomposition dynamics of copper oxide by nanocalorimetry-coupled time-of-flight mass spectrometry, *Chem Phys Lett*, **2017**, *689*, 26-29. doi: 10.1016/j.cplett.2017.09.066.

[32] I. Abdallah, J. Zapata, G. Lahiner, B. Warot-Fonrose, J. Cure, Y. Chabal, A. Esteve, C. Rossi, Structure and Chemical Characterization at the Atomic Level of Reactions in Al/CuO Multilayers, *ACS Applied Energy Materials*, **2018**, *1* (4), 1762–1770. doi: 10.1021/acsaem.8b00296.

[33] I. Monk, M. Schoenitz, R. J. Jacob, E. L. Dreizin, M. R. Zachariah, Combustion Characteristics of Stoichiometric Al-CuO Nanocomposite Thermites Prepared by Different Methods, *Combust Sci Technol*, **2017**, *189* (3), 555-574. doi: 10.1080/00102202.2016.1225731.

[34] K. T. Sullivan, W. A. Chiou, R. Fiore, M. R. Zachariah, In situ microscopy of rapidly heated nano-Al and nano-Al/WO3 thermites, *Appl Phys Lett*, **2010**, *97* (13). doi: 10.1063/1.3490752.

[35] S. M. Umbrajkar, M. Schoenitz, E. L. Dreizin, Exothermic reactions in Al-CuO nanocomposites, *Thermochim Acta*, **2006**, *451* (1-2), 34-43. doi: 10.1016/j.tca.2006.09.002.

[36] G. K. Batchelor and R. W. O'Brien, Thermal or electrical conduction through a granular material, *Proc. R. Soc. Lond.,**1977**, A355 (1682)* 313–333. doi:10.1098/rspa.1977.0100.

[37] M. Moscardini, Y. Gan, S. Pupeschi, M. Kamlah, Discrete element method for effective thermal conductivity of packed pebbles accounting for the Smoluchowski effect. *Fusion Engineering and Design*, *127*, 192–201. doi: 10.1016/j.fusengdes.2018.01.013.

[38] M.N. Ozisik, *Heat transfer: a basic approach*. New York: McGraw-Hill, 1985.

[39] L. Catoire, J. F. Legendre, M. Giraud, Kinetic model for aluminum-sensitized ram accelerator combustion, *J Propul Power*, **2003**, *19* (2), 196-202. doi: 10.2514/2.6118.

[40] D. G. Goodwin, R. L. Speth, H. K. Moffat, B. W. Weber, Cantera: An Object-oriented Software Toolkit for Chemical Kinetics, Thermodynamics, and Transport Processes Version 2.5.1 (2021).

[41] J. Glorian, S. Gallier, L. Catoire, On the role of heterogeneous reactions in aluminum combustion, *Combust Flame*, **2016**, *168*, 378-392. doi: 10.1016/j.combustflame.2016.01.022.

[42] J. Malcolm W. Chase, NIST-JANAF thermochemical tables, Fourth edition. Washington, DC : American Chemical Society ; New York : American Institute of Physics for the National Institute of Standards and Technology, 1998.

[43] B. J. McBride, NASA Glenn coefficients for calculating thermodynamic properties of individual species. (National Aeronautics and Space Administration, John H. Glenn Research Center …, 2002).

[44] L. Zhou, N. Piekiel, S. Chowdhury, M. R. Zachariah, Time-Resolved Mass Spectrometry of the Exothermic Reaction between Nanoaluminum and Metal Oxides: The Role of Oxygen Release, *J Phys Chem C*, **2010**, *114* (33), 14269-14275. doi: 10.1021/jp101146a.

[45] J. Kwon, J. M. Ducere, P. Alphonse, M. Bahrami, M. Petrantoni, J. F. Veyan, C. Tenailleau, A. Esteve, C. Rossi, Y. J. Chabal, Interfacial Chemistry in Al/CuO Reactive Nanomaterial and Its Role in Exothermic Reaction, *Acs Appl Mater Inter*, **2013**, *5* (3), 605-613. doi:10.1021/am3019405.

[46] M. L. Pantoya, J. J. Granier, Combustion behavior of highly energetic thermites: Nano versus micron composites, *Propell Explos Pyrot*, **2005**, *30* (1), 53-62. doi: 10.1002/prep.200400085.

[47] M. Bahrami, G. Taton, V. Conedera, L. Salvagnac, C. Tenailleau, P. Alphonse, C. Rossi, Magnetron Sputtered Al-CuO Nanolaminates: Effect of Stoichiometry and Layers Thickness on Energy Release and Burning Rate, *Propell Explos Pyrot*, **2014**, *39* (3), 365-373. doi: 10.1016/j.combustflame.2019.04.031.

[48] G. Lahiner, A. Nicollet, J. Zapata, L. Marín, N. Richard, M.D. Rouhani, C. Rossi, A. Esteve, A diffusion–reaction scheme for modeling ignition and self-propagating reactions in Al/CuO multilayered thin films, *Journal of Applied Physics*, **2017,** *122*, 155105. Doi: 10.1063/1.5000312.